iScience

CellPress

Article

Tracking Newly Released Synaptic Vesicle Proteins at Ribbon Active Zones

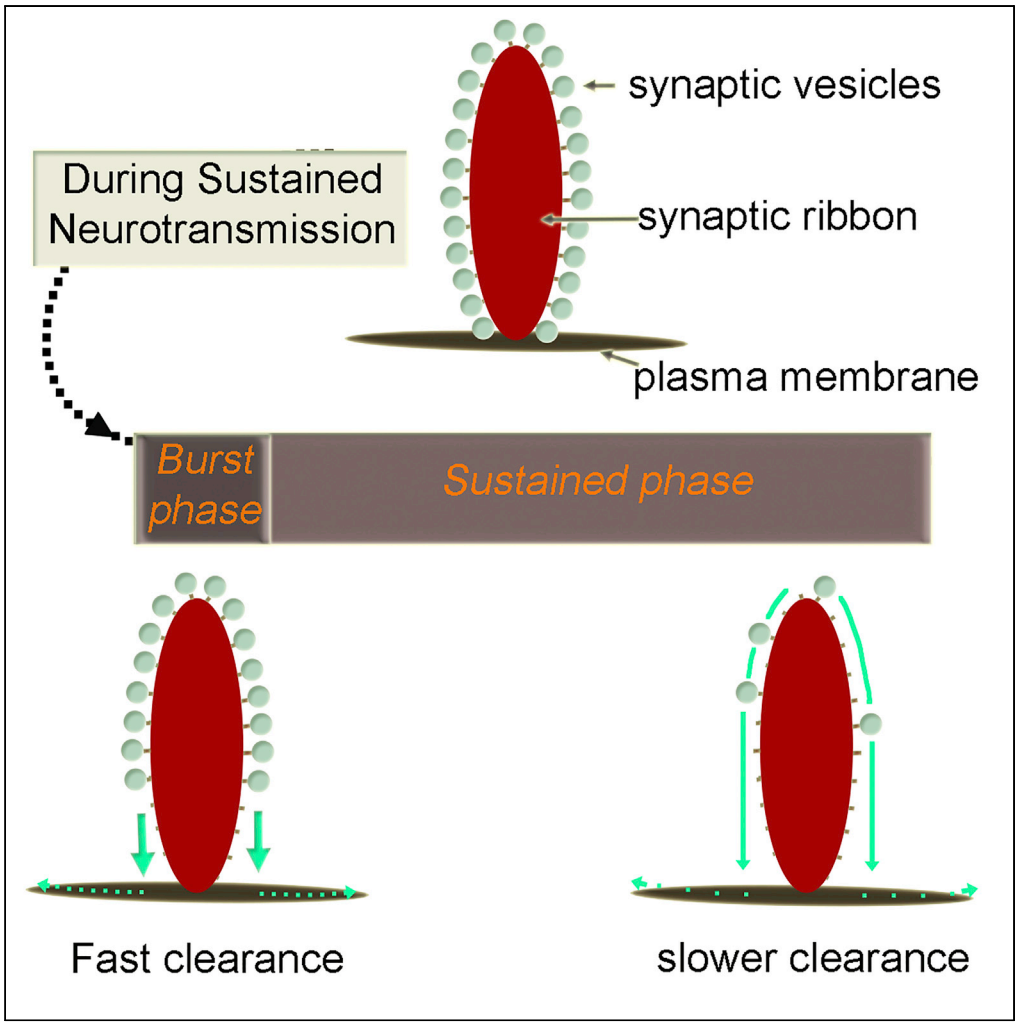

Thirumalini Vaithianathan, Lonnie P. Wollmuth, Diane Henry, David Zenisek, Gary Matthews

tvaithia@uthsc.edu

HIGHLIGHTS

We monitor single-molecule clearance after exocytosis in ribbon synapses of zebrafish

Diffusion of synaptophysin is dependent on the time and localization of fusion events

Synaptophysin diffusion is slower than reported in other systems

Bipolar cell synapses may not be rate limited by protein clearance after exocytosis

Vaithianathan et al., iScience *17*, 10–23
July 26, 2019
https://doi.org/10.1016/j.isci.2019.06.015

iScience

CellPress

Article

Tracking Newly Released Synaptic Vesicle Proteins at Ribbon Active Zones

Thirumalini Vaithianathan,[1,7,8,*] Lonnie P. Wollmuth,[1,2,3] Diane Henry,[1] David Zenisek,[5,6] and Gary Matthews[1,4]

SUMMARY

Clearance of synaptic vesicle proteins from active zones may be rate limiting for sustained neurotransmission. Issues of clearance are critical at ribbon synapses, which continually release neurotransmitters for prolonged periods of time. We used synaptophysin-pHluorin (SypHy) to visualize protein clearance from active zones in retinal bipolar cell ribbon synapses. Depolarizing voltage steps gave rise to small step-like changes in fluorescence likely indicating release of single SypHy molecules from fused synaptic vesicles near active zones. Temporal and spatial fluorescence profiles of individual responses were highly variable, but ensemble averages were well fit by clearance via free diffusion using Monte Carlo simulations. The rate of fluorescence decay of ensemble averages varied with the time and location of the fusion event, with clearance being most rapid at the onset of a stimulus when release rate is the highest.

INTRODUCTION

Ribbon synapses of sensory neurons support continuous exocytosis in response to sustained depolarization (Matthews and Fuchs, 2010). To support the continuous release of neurotransmitters, rapid replenishment of release-ready synaptic vesicles at presynaptic active zones is required. At conventional, non-ribbon-type synapses, clearance of fused synaptic vesicle proteins from the release site is an important determinant of recovery from short-term synaptic depression, and the clearance and availability of release sites has been suggested to be rate limiting during sustained synaptic release (Hosoi et al., 2009; Hua et al., 2013; Neher, 2010; Rajappa et al., 2016; Wu et al., 2009). Furthermore, at rod ribbon synapses, maintenance of endocytosis, which is an important mechanism to clear synaptic vesicle proteins, is required to maintain release even at moderate frequencies (Wen et al., 2018). Therefore, clearance of release sites may be of great importance during sustained release at ribbon synapses.

To study protein clearance following exocytosis, we took advantage of a line of zebrafish, which weakly express the exocytosis reporter, SypHy (synaptophysin-pHluorin fusion protein), a transgene driven by the HSP70 promoter (Vaithianathan et al., 2016). Increase in SypHy fluorescence in response to stimulation reports exocytosis, when the interior of the vesicle connects with the external medium (Sankaranarayanan et al., 2000). By using a weakly expressing line, we can monitor the fate of individual molecules following exocytosis with high spatial and temporal precision. To localize fusion of single vesicles and trafficking of synaptophysin after fusion, we imaged vesicle trafficking at the active zone of bipolar cell ribbon synapses at high spatial resolution (Vaithianathan et al., 2016). In this study, imaging of single SypHy molecules using rapid confocal line scans reveals a decay in fluorescence, largely reflecting lateral movement of synaptophysin molecules out of the imaging locale. In addition, our results indicate that when and where a fusion event occurs correlates with the amount of time the synaptophysin molecule resides in the imaging region, with clearance being accelerated at times when exocytosis rates are the highest.

RESULTS

To track the dynamics of a fused vesicle protein, we used transgenic zebrafish expressing SypHy under control of a heat shock promoter (Vaithianathan et al., 2016). SypHy is essentially nonfluorescent when the fluorophore is contained within the acidic environment of a synaptic vesicle (Balaji and Ryan, 2007; Granseth et al., 2006; Sankaranarayanan et al., 2000; Voglmaier et al., 2006; Wu et al., 2009), but rapidly becomes fluorescent upon exocytosis as it deprotonates. Hence, SypHy is a reliable marker of plasma-membrane synaptophysin localization following exocytosis. We specifically chose low-expressing SypHy transgenic zebrafish for the following reasons: (1) low-expressing cells are less prone to overexpression artifacts, such as saturation of membrane retrieval mechanisms, and thus may more reliably report endogenous protein

[1]Department of Neurobiology and Behavior, Stony Brook University, Stony Brook, NY 11794, USA

[2]Center for Nervous System Disorders, Stony Brook University, Stony Brook, NY 11794, USA

[3]Department of Biochemistry & Cell Biology, Stony Brook University, Stony Brook, NY 11794, USA

[4]Department of Ophthalmology, Stony Brook University, Stony Brook, NY 11794, USA

[5]Department of Cellular and Molecular Physiology, Yale University School of Medicine, New Haven, CT 06520-8066, USA

[6]Department of Ophthalmology and Visual Sciences, Yale University School of Medicine, New Haven, CT 06520-8066, USA

[7]Present address: Department of Pharmacology, College of Medicine, The University of Tennessee Health Science Center, 71 South Manassas St., Memphis, TN 38163, USA

[8]Lead Contact

*Correspondence: tvaithia@uthsc.edu

https://doi.org/10.1016/j.isci.2019.06.015

behavior and (2) overexpression may lead to excess surface expression (Royle et al., 2008), reducing the likelihood of detecting individual molecules at high spatial and temporal resolution.

Retinal bipolar cells contain vesicle-binding scaffolds, known as synaptic ribbons, which localize vesicles to active zones. Synaptic ribbons are made up largely of the protein Ribeye. In this study, synaptic ribbons were labeled with a fluorescent peptide that binds to Ribeye (CF-633-RBP) (Vaithianathan et al., 2016; Zenisek et al., 2004) delivered via a patch pipette placed directly on a bipolar terminal (Figure 1A, left). SypHy fluorescence was monitored by line scan confocal imaging along the length of the synaptic ribbon in a direction perpendicular to the plasma membrane (Figure 1A, right). To evoke exocytosis, the membrane potential was stepped to −10 mV for 1 s from a resting potential of −60 mV (Figure 1B, red line), where we measured both membrane current (Figure 1B) and capacitance (not shown). From these line scans, we derived the spatial (Vaithianathan and Matthews, 2014) (Figure 1C) and temporal (Figure 1D) aspects of SypHy fluorescence relative to the synaptic ribbon and plasma membrane.

Spatial Aspects of SypHy Fluorescence Report Locus of Synaptic Vesicle Fusion Relative to a Single Ribbon Active Zone and the Plasma Membrane

To determine the locus of vesicle fusion, we analyzed the x axis profiles of SypHy fluorescence relative to a synaptic ribbon and the plasma membrane (Figure 1C) (Vaithianathan et al., 2016). For consistency, we display line scans such that the outside of the cell is to the right. Although SypHy fluorescence was detectable in individual scan lines, the low signal relative to noise precluded accurate localization. We therefore averaged line scans over 2 pixels in the x axis and 5–8 lines in the t-axis (Figure S1 and Methods). The fluorescence intensity profile of SypHy events perpendicular to the membrane was then analyzed to determine the position of SypHy events relative to the ribbon and the plasma membrane (Figure 1C). A histogram of the x axis position of 81 SypHy events (Figure S2) indicates that as reported previously (Vaithianathan et al., 2016) they were broadly spread across the ribbon and were not confined to positions near the plasma membrane.

Characterization of Individual pHluorin Events

Depolarization of bipolar cells occasionally gave rise to events, characterized by rapid increases in fluorescence above baseline followed by a slower decay that we took to represent the exocytosis of a single vesicle (see below). To track the dynamics of such SypHy fusion events, we analyzed SypHy fluorescence in time relative to the stimulating voltage step (Figure 1D). SypHy signals appeared abruptly as expected for the nearly instantaneous loss of vesicle protons upon fusion and persisted for some time before declining to baseline fluorescence (Figure 1D, lower panel) indicating movement of the SypHy molecule out of the x-t line scan, endocytosis followed by reacidification, or photobleaching.

x-t line scans were obtained from 1,453 ribbons during sustained depolarization (Figure 2). We identified SypHy events in 81 of these recordings and characterized their amplitude (e.g., Figure 2A) (see Methods). The majority of line scans (1,372) exhibited no detectable events (e.g., Figure 2B), which we refer to as "null" events. It is possible that there are errors in the distinction between SypHy and null events, but we think these errors are minimal for several reasons: first, we characterized the baseline or imaging noise in the absence of a stimulus (Figure 2C, inset). This distribution was well fit by a Gaussian (red line) with an average amplitude of −0.4 a.u. and an SD of 4.9 (N = 36). The average amplitude of presumed SypHy events (27.1 ± 1.2 a.u., N = 81) (Figure 2C, green bars) far exceeds this noise level with the bulk of the events having amplitudes >1.5 SD. Second, to characterize the amplitude of presumed null recordings, we randomly selected 203 recordings without detectable events and measured the amplitude right after the voltage step (Figure 2C, gray bars). These amplitudes were well fit by a Gaussian function with parameters (average amplitude of −0.6 a.u., SD of 4.0, N = 203) comparable to the imaging noise, consistent with these nulls arising from noise. Third, to test for whether there could be hidden SypHy events in the noise of presumed null events, we averaged the 203 randomly selected events by aligning them to the start of the depolarization, when exocytic rate is the highest (Figure 2B, inset). If we are consistently missing events beneath the noise floor, signal averaging across many traces would reduce the noise and reveal this signal. However, no dramatic changes in fluorescence occurred from baseline, arguing against a significant contribution from hidden SypHy events. Finally, we also compared events of low and high amplitudes to see if they behave similarly or not (Figure S4), with the idea that multiple simultaneous events, which would most likely occur with the brighter events, would behave differently. However, we saw no difference (Figure S4), arguing against any fundamental difference between small and large events.

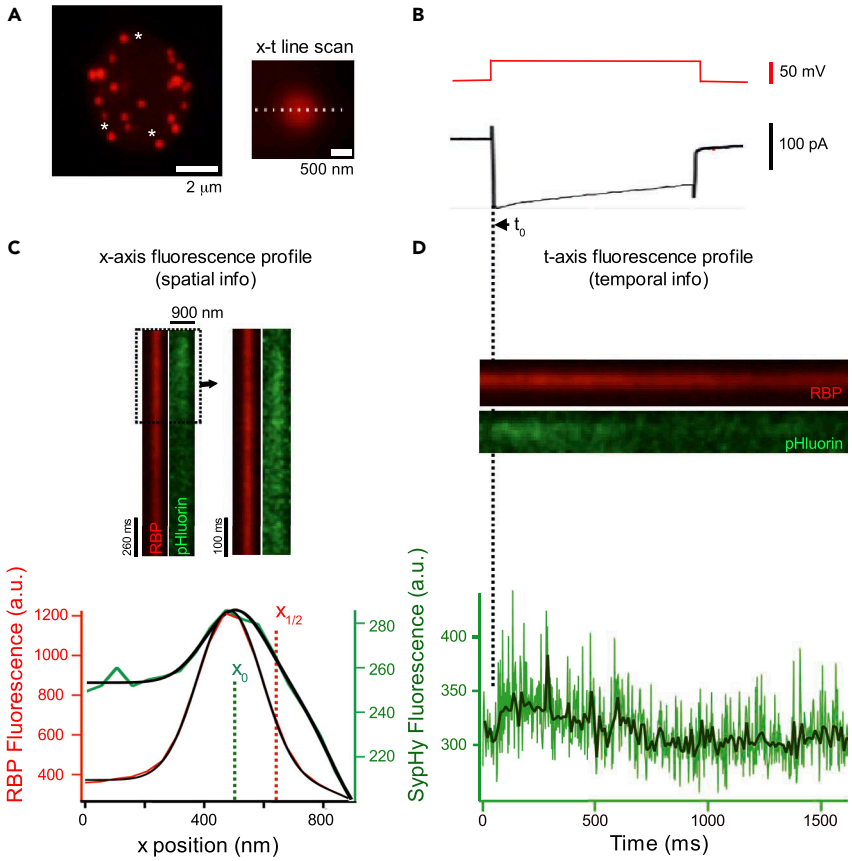

Figure 1. High-Resolution Imaging of SypHy Fluorescence Reports Spatiotemporal Aspects of Synaptic Vesicle Fusion at a Single Ribbon Active Zone

(A) Overview of experimental procedure. (Left) 2D projection from a series of confocal optical sections through a zebrafish bipolar cell synaptic terminal. A synaptic terminal was voltage clamped using a whole-cell pipette with an internal solution containing deep-red-fluorescent RBP (CF633-RBP) to label synaptic ribbons. RBP fluorescence was concentrated at ribbons and also filled the entire terminal, which allowed visualization of the terminal border. Experiments were carried out on ribbons that could be distinguished from adjacent ribbons (e.g., white asterisks). (Right) Close-up view of a single synaptic ribbon. The outside of the cell is to the right, which is the standard orientation adopted for all images. x-t scan lines (broken line) were positioned perpendicular to the plasma membrane, extending from the intracellular side of the ribbon to the extracellular space. These x-t raster plots were used to measure the fluorescence intensity profiles of RBP (red) and SypHy (green) shown in (C and D).

(B) Voltage-clamp recording of a bipolar cell terminal. Terminals were held at −60 mV and stepped to −10 mV (t_0) for 1 s (red) to evoke a sustained Ca^{2+} current (black). Logic pulses exchanged between patch-clamp and imaging computers synchronized acquisition of x-t line-scan and imaging data. A typical experiment begins with voltage command (V_H = −60 mV); a transistor-transistor logic (TTL) pulse generated from Patch Master triggers image acquisition. t_0 is the time of depolarization (see Methods).

(C) Illustration of the approach to obtain the spatial location of SypHy fluorescence with respect to the ribbon. (Top) Example of an x-t raster plot oriented to illustrate x axis intensity profiles of RBP (red) and SypHy (green) fluorescence during sustained depolarization. (Bottom) Fluorescence intensity profiles along the x axis for RBP (red) and SypHy (green) were fit with a sigmoid Gaussian function (see Methods) (Vaithianathan et al., 2016). The centroid (x axis position) of RBP and SypHy was taken as the peak of the Gaussian fit (x_0, shown by dotted green line for SypHy). The parameter $x_{1/2}$ (dotted red line) from the sigmoid fit to the RBP fluorescence (red trace) was used to estimate the location of the plasma membrane.

(D) (Top) x-t raster plot, same recording as in (C) but reoriented to demonstrate t axis intensity profiles of RBP (red) and SypHy (green) fluorescence during sustained depolarization. Scans were averaged over 5 pixels. (Bottom) Raw (light green) or averaged (black line) temporal intensity profile of the SypHy fluorescence over a region of interest (see also Figure S1).

See also Figures S1 and S2.

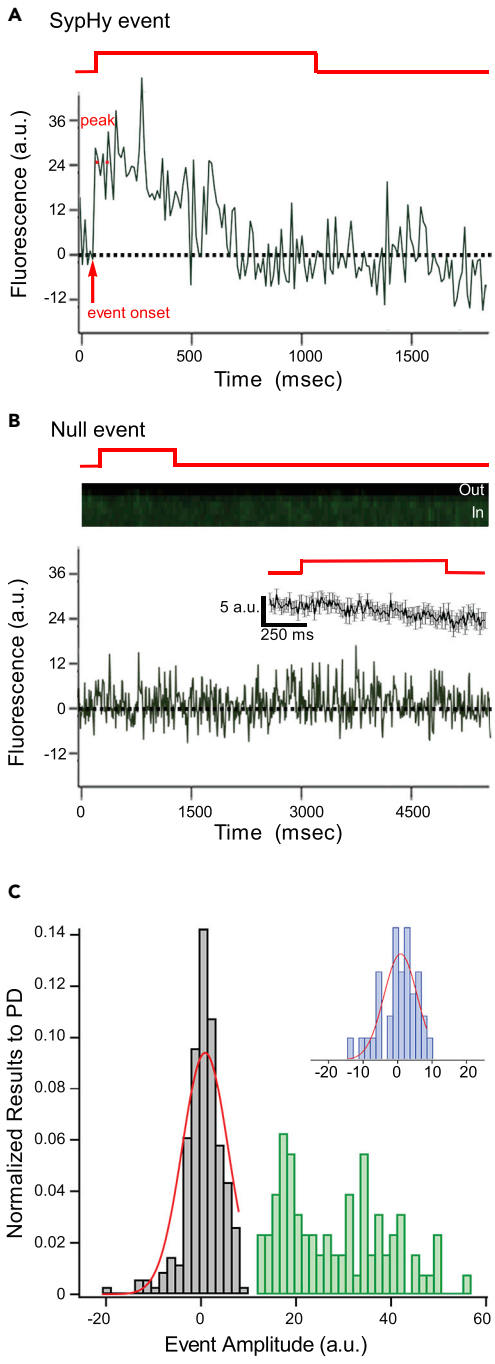

Figure 2. SypHy Fluorescence Reports Single Fusion Events

(A and B) Examples of averaged temporal intensity profile (see Figure S1) of green fluorescence illustrating the occurrence of either an SypHy (A) or a null (B) event. For analysis and display, fluorescence was normalized to baseline fluorescence before the depolarization. Detection of SypHy events and analysis of amplitudes were determined as explained in Methods. Briefly, events were visually identified from x-t scans, and only events with $\geq$1.5 SDs above the average amplitude of baseline noise (see Figure 2C, inset) were defined as SypHy events. Depolarizations that failed to elicit an identifiable event were defined as "null" events (B). (B, inset) Ensemble of 203 randomly chosen null events (see panel C, gray bars). The voltage protocols (red) indicate the timing of the depolarization. For all recordings, including null events, capacitance measurements with sustained depolarization reported strong increases in capacitance (~150 fF) indicating robust exocytosis.

(C) Histogram showing distribution of event amplitudes for null and SypHy events. Amplitudes were measured for 203 randomly selected nulls (out of 1,372 nulls total) (see Methods). The results (gray bars) were normalized to the total number of nulls (probability density). The average amplitude of null and SypHy events were −0.6 $\pm$ 0.3, N = 203, and 27.1 $\pm$ 1.2, N = 81, respectively. The distribution of null amplitudes is well fit (red line) by the same Gaussian function that defines the noise (i.e., in the absence of a stimulus) (inset) with the amplitude as the only free parameter. (Inset) Histogram of fluorescence changes, ΔF, in the absence of stimulation provides the baseline variability, the imaging noise. Baseline noise fluorescence was obtained using the same approach as with SypHy and nulls, except that noise measurements were made in the absence of a stimulus (see Methods). The results were normalized to the total number of trials and fit with Gaussian function in red (σ = 4.9) (noise average amplitude: −0.4 $\pm$ 0.9; N = 36).

See also Figures S3 and S4.

Three observations suggest that SypHy fluorescence events predominantly represent the dequenching of a single pHluorin molecule following exocytosis. First, SypHy events occurred infrequently, only in 5.6% of all trials (81 SypHy events in 1,453 line scans). If one assumes a random distribution of SypHy molecules across all ribbons in this study, then the likelihood of two molecules being liberated during a single voltage step would be 0.3% ($.056^2$). In 1,453 trials, we expect that this would happen about five times. Second, of the 81 SypHy events, six occurred before (one event) or long after (five events) the voltage step at a time when fusion events are rare (e.g., Figures S3A and 3C) and thus likely reflect a single vesicle. The average amplitude of evoked SypHy events (27.1 $\pm$ 1.2, N = 75) is indistinguishable from that for these rare events (25.2 $\pm$ 4.9, N = 6) (Figure S3B). Third, the point-spread function (PSF), quantified by the full width at half

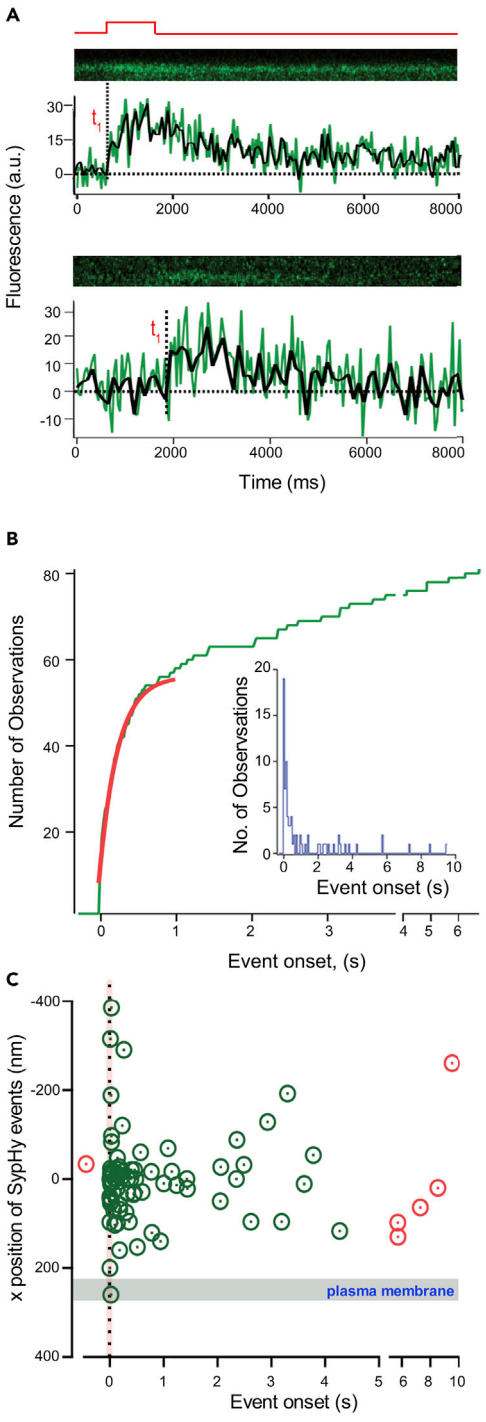

Figure 3. SypHy Events Report Two Components of Vesicle Fusion

(A) Examples of SypHy events occurring at different times following depolarization. Event onset (dashed lines, t_1) was the time when the SypHy fluorescence reached 10% of the event amplitude. (Upper trace) SypHy event onset (1–2 ms) just after the start of depolarization. (Lower trace) SypHy event onset occurred around 1,220 ms after the start of depolarization. The voltage protocol shown at the top (red) is for both recordings.

(B) Cumulative distribution of SypHy event onsets (green) up to 5 s after the start of depolarization (N = 75). The red line is a double exponential fitted to time constants of the fast to slow component of capacitance measurements for zebrafish retinal bipolar cells, τ_{fast} = 2.3 ms and τ_{slow} = 162 ms (Mennerick and Matthews, 1996; Vaithianathan and Matthews, 2014; von Gersdorff and Matthews, 1994). The resulting ratio of the fast to slow component of capacitance measurements (1:6) is similar to that obtained for zebrafish bipolar cells (1:5). (Inset) Histogram of the event onset of the 81 SypHy events.

(C) x axis position of SypHy events with respect to ribbon PSF (Figure S2) plotted against their event onset. The location of plasma membrane (gray shading) and centroid (x axis) position of SypHy was estimated using sigmoid-Gauss function (see Methods; Figure 1C).

Early events, those occurring within 30 ms of depolarization (red shading), occurred both proximal and distal to the plasma membrane (Vaithianathan et al., 2016). SypHy events that occurred up to 4 s after the end of the voltage step (shown in green) were defined as evoked events, whereas SypHy events that occurred before the stimulus or more than 4 s after the end of voltage step are classified as rare (show in red, N = 6).

maximum (FWHM), of a diffraction-limited 27-nm fluorescence bead (Figure S3C) matches the FWHM of SypHy fluorescence obtained in line scans imaged under the same imaging parameters (Figure S3D).

Because we relate the rate of decline detected in temporal aspects of SypHy fluorescence (Figure 1D, lower panel) to movement of the SypHy molecule from fusion sites, one concern could be stability in tracking the SypHy fluorescence due to drift and photobleaching. However, bleaching rate was minimal during the time course of a typical experiment and accounts for less than 17% with a time constant of

1.8 ± 0.2 s (N = 3) evaluated from line scans obtained from immobilized GFP under the same imaging parameters (data not shown). On average ribeye-binding peptide (RBP) fluorescence was stable over time during an imaging session (data not shown).

Rate of SypHy Events Occurrence Correlates to Kinetic Components of Bipolar Cell Ribbon Synapses' Exocytosis

Bipolar cell ribbon synapses exhibit two kinetically distinct components of transmitter release in response to step depolarizations: a phasic component that consists of a limited pool of vesicles that can be tapped rapidly but is also rapidly exhausted, generating a transient spike of release, and a tonic component that comprises a much larger pool of more slowly released vesicles (Mennerick and Matthews, 1996; Vaithianathan and Matthews, 2014; von Gersdorff and Matthews, 1994).

The majority of SypHy events occurred soon after the start of membrane depolarization (Figure 3A, upper trace), whereas other events occurred after a delay (Figure 3A, lower trace). To test whether the timing of SypHy events agreed with the known time course of bipolar ribbon synapse transmitter release, we determined the time of onset of SypHy events, relative to the start of membrane depolarization, and plotted them as a cumulative distribution (Figure 3B) and frequency histogram (Figure 3B, inset). We fit the cumulative histogram of event onsets with known kinetic components of release from capacitance measurements for zebrafish and goldfish retinal bipolar cells, τ_{fast} = 2.3 ms and τ_{slow} = 162 ms (Mennerick and Matthews, 1996; Vaithianathan and Matthews, 2014; von Gersdorff and Matthews, 1994). The resulting amplitude-ratio of the fast to slow component of capacitance measurements (1:6) is comparable with measurements obtained for bipolar cells (1:5). These results are consistent with individual SypHy events representing fusion of single vesicles.

We next compared the time of vesicle fusion relative to its location on the ribbon (Figure 3C). Our results show that during the burst phase of vesicle fusion that occurs within 30 ms after the onset of stimulation (Figure 3C, red shading) most events were in the half of the ribbon that was proximal to the plasma membrane (Figure 3C, gray shading). However, there were events also localized distal to the plasma membrane (Figure 3C, negative values). Similarly, SypHy events that occurred after 500 ms of onset of stimulation also had fusion events both proximal and distal to the plasma membrane. These results infer that during sustained stimulation there is no obvious relationship between the timing of events and their location.

Dynamics of SypHy Fusion Events at a Single Ribbon

SypHy signals increased abruptly but remained elevated for some time before returning to baseline (Figure 4). To quantify this SypHy dwell time or event duration, we measured from event onset (red arrow) to when fluorescence decayed to 1σ (68.3%) of the event amplitude (shaded green, Figure 4A) (see Methods). Dwell times were approximately exponentially distributed (Figure 4B) with a time constant of 340 ms. The fluorescence decay of individual SypHy events varied considerably, as expected for the behavior of individual molecules acting stochastically. To analyze the properties of SypHy clearance from the line scan, we averaged SypHy events (N = 81) aligned to the start of event onset (Figure 5A) (see Methods). The decay phase of the averaged SypHy events was roughly exponential with τ = 470.7 ± 99.2 ms. The decay in fluorescence may represent diffusion out of the line scan, photobleaching, or internalization and reacidification. However, the contribution of photobleaching (1.8 ± 0.2 s; 17%) is 5-fold slower than the decay rate (see Methods).

To estimate the possible contribution of endocytosis and reacidification of SypHy molecules to the decay of the signal, we looked at SypHy fluorescence across the entire synaptic terminal with a maximally expanded pinhole to assay fluorescence throughout the terminal (Figure 5B). For these experiments we used a highly expressing SypHy fish (see Methods). By visualizing the entire surface-exposed pool, diffusion should not contribute to the decay in fluorescence, but instead reflects a combination of internalization, acidification, and photobleaching. The decay in the SypHy signals was well fit by a single exponential (Figure 5B, red line). Experiments done on individual ribbons showed a decay time of 15.0 ± 3.5 s (N = 27 SypHy) (Figure 5B, inset). Given that this is much slower than the line scan decay time (about 470 ms) (Figure 5A), this suggests that the fluorescent decay of the individual SypHy events predominantly reflects diffusion out of the small line scan region rather than internalization or photobleaching. Hence, we interpret the individual events as exocytosis liberating single SypHy molecules,

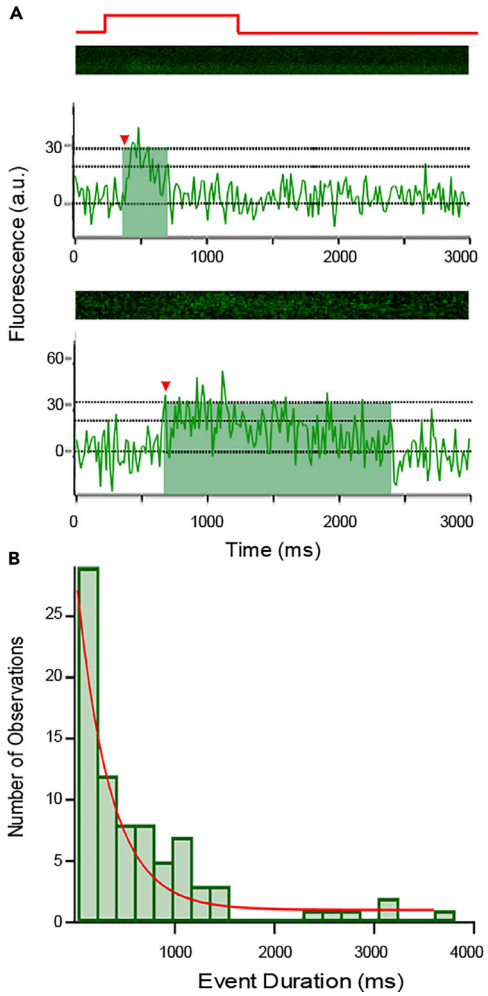

Figure 4. SypHy Fluorescence Persists at the Active Zone after Fusion

(A) Examples of x-t scans of SypHy events illustrating variations in the duration of SypHy fluorescence. In some instances, SypHy events were brief (e.g., upper recording), whereas in other instances they persisted longer (e.g., lower recording). To quantify SypHy dwell time or event duration, we measured from event onset (red arrow) to when fluorescence decayed to 1σ (68.3%) of the event amplitude (green shades) (see Methods). Temporal intensity profile is the same as in Figure 1D. We assume the event duration reflects how long the SypHy molecule lingers within the line scan.

(B) Histogram of event durations (N = 81 SypHy events) is approximately exponentially distributed, with a time constant of 340 ms.

followed by diffusion of the fluorescent molecule out of the line scan, where it gradually becomes less fluorescent as it moves away.

Dynamics of SypHy Clearance

To begin to address the dynamics of clearance from ribbon synapse active zones, we initially considered timing of fusion events. Bipolar terminals show two kinetically distinct components, a fast-transient phase at the beginning of depolarization and a slow-sustained phase occurring at later times. Vesicle clearance during these phases might be quite different owing to the near-simultaneous insertion of significant amounts of vesicle membrane into a confined space, which could either push membrane out of the synaptic region or crowd the active zone plasma membrane with vesicle components.

To define the impact of timing on vesicle clearance, we compared time courses for ensemble averages of SypHy events occurring within 30 ms or 0.5 s after onset of depolarization (Figure 6) (see Methods). We refer to these components as burst (30 ms) or sustained-phase (0.5 s after) events. We found that the dwell time

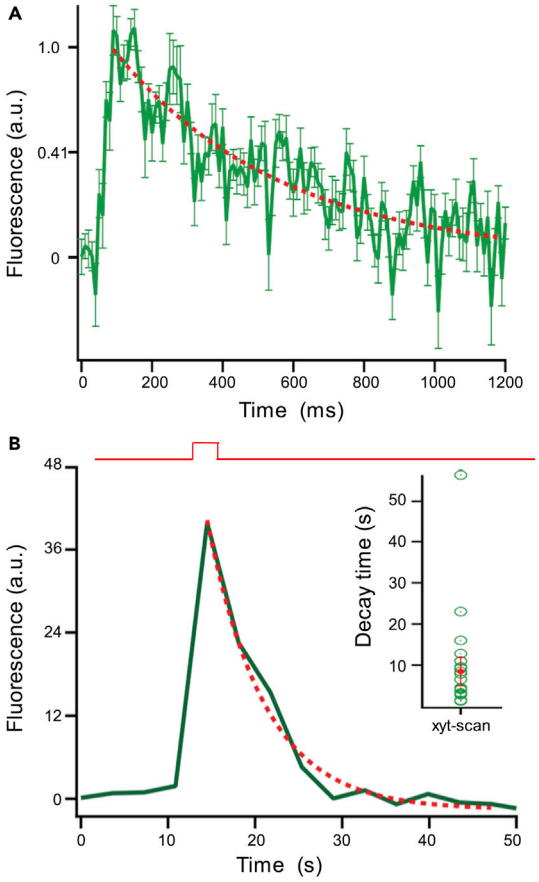

Figure 5. High-Resolution Imaging of a Single SypHy Molecule Reports a Fast Decay Component Attributed to Lateral Movement of Fused Vesicle Protein

(A) Ensemble SypHy events (N = 81) from x-t line scans. x-t scans sampled at different rates were interpolated to a common time base (10-ms sample interval) using the interpolation function in Igor. Scans were aligned to event onset and normalized to their event amplitude.

The decay phase of the average SypHy event was well fit with an exponential function with τ = 470.7 $\pm$ 99.2 ms (N = 81).

(B) Example of SypHy fluorescence from an x-y scan taken from a bipolar terminal from highly expressing SypHy fish with a maximally expanded pinhole to assay fluorescence throughout the terminal. Voltage step is shown above. The recovery phase, which presumably reflects the time for internalization, acidification, and photobleaching, was exponential with τ = 4.3 s. In x-y scans (inset) of a square region of interest of 1 × 1 μm centered over a single terminal, recovery of SypHy florescence occurs with a median of 15.0 $\pm$ 3.5 s (N = 27 recordings from 12 different terminals).

of the ensemble averages was briefer for burst events compared with sustained-phase events (Figures 6A and 6B, green shading) (300 ms versus 700 ms).

To test whether diffusion could explain the decay rate for ensemble SypHy events, we used a Monte Carlo model (see Methods). Briefly, we simulated individual molecules undergoing a random walk in two dimensions, both perpendicular to the axis of the ribbon, one in the z axis and one in the y axis. The fluorescence intensity of the molecule was determined by its distance from the center of the axis of the line scan convolved by the PSF of the microscope, measured with a sub-diffraction limited bead, taking into account the differences in PSF in the z plane and the x/y plane. The only free parameter in the simulation was the diffusion coefficient of the simulated molecules (i.e., step size), which was allowed to vary to best fit the data. For each condition, 84 single molecules were simulated. The diffusion coefficient was varied to obtain a best fit to the data (green lines, Figures 6C and 6D). Burst events were best fit by a diffusion coefficient of 41.8 nm^2/ms, whereas sustained events were best fit with a diffusion coefficient of 9.6 nm^2/ms. Thus, during burst events SypHy molecules diffuse out of the active zone more rapidly than during periods of sustained release, an effect possibly related to the total amount of membrane added.

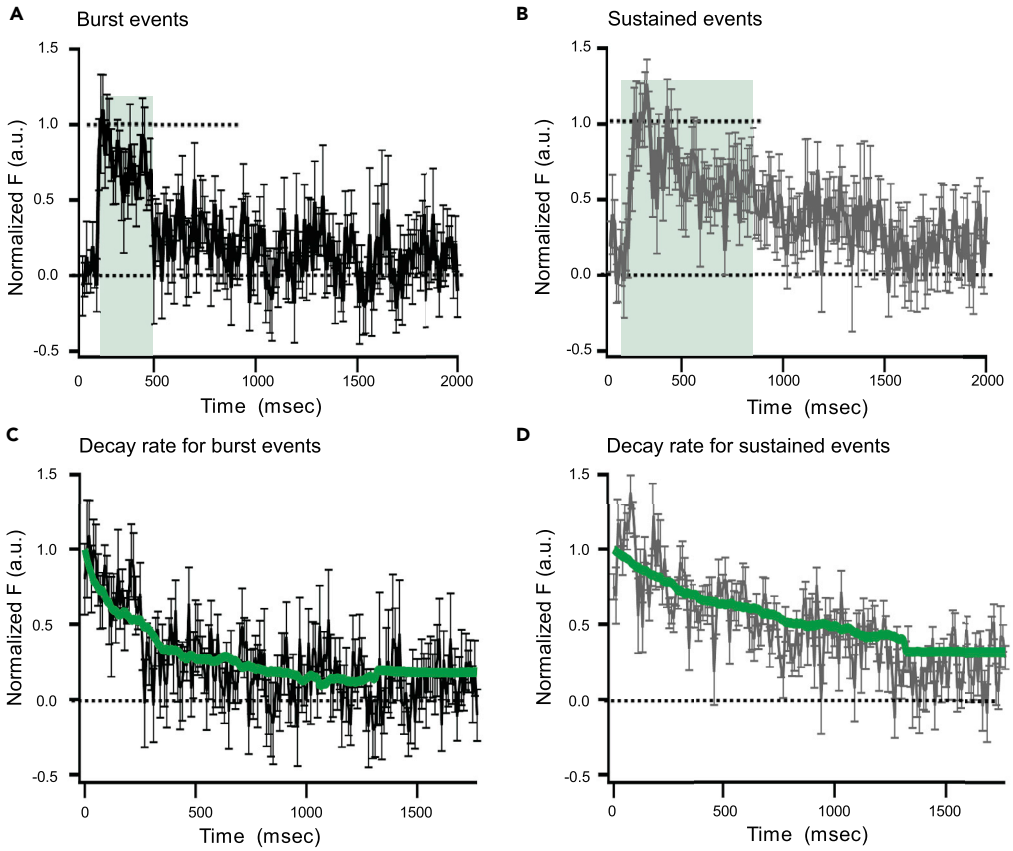

Figure 6. Kinetics of SypHy Events Occurring Early or Late Following the Onset of Depolarization

(A and B) Ensemble of SypHy events occurring within 30 ms (A, N = 16, referred to as "burst" events) or after 0.5 s (B, N = 57, referred to as "sustained" events) after the onset of depolarization. SypHy events occurring early in the depolarization or burst events (A) appeared abruptly, remained at a constant level (~300 ms, green shading), and then declined. SypHy events occurring late in depolarization or sustained events (B) persist longer compared with burst events (~700 ms, green shading), before decaying. For comparison, fluorescence was normalized to the peak for the individual record (see Methods).

(C and D) Decay of ensemble SypHy fluorescence for burst (black, C) or sustained (gray, D) events. We performed Monte Carlo simulations (2D random walk) of diffusional clearance of SypHy from the active zone to compare clearance rates for burst or sustained events (see Methods). The diffusion coefficient was varied to obtain a best fit to the data (green lines). Burst events were best fit by a diffusion coefficient of 41.8 nm^2/ms, whereas sustained events were best fit with a diffusion coefficient of 9.6 nm^2/ms.

Clearance of SypHy Molecules Depends upon the Location of Fusion

Vesicle fusion occurred at different locations relative to the plasma membrane (Figure 7). To test whether the location of the fusion event influenced the rate of clearance from the active zone, we grouped SypHy events based on the location relative to the center of the ribbon in the x dimension (x_0 defined above); SypHy events that occurred at $x_0 > 50$ nm and $x_0 < -50$ nm were classified as membrane proximal and distal events, respectively. Proximal SypHy events show faster kinetics compared with distal events, where dwell times of proximal events were twice faster than those of the distal events (Figures 7A and 7B) (~300 ms versus > 700 ms) and the apparent diffusion coefficient estimated with best-fit Monte Carlo simulation resulted in a diffusion coefficient of 49 nm^2/ms for proximal events and 16.1 nm^2/ms for distal events.

SypHy Diffusion at Extrasynaptic Locations

The experiments above addressed movement of recently released SypHy molecules in the restricted area of the synapse. A key question is whether SypHy mobility is different in this restricted environment than in the rest of the synaptic terminal. To address this question, we performed fluorescence recovery after

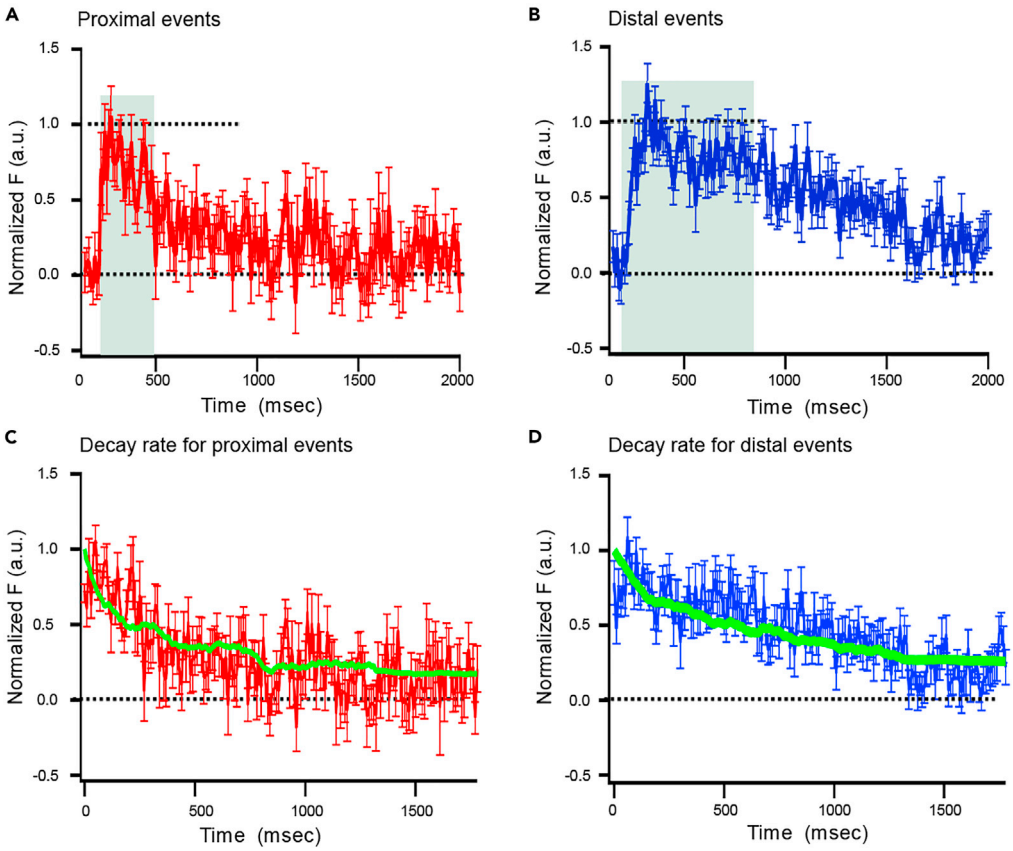

Figure 7. Kinetics of SypHy Events Occurring at Membrane Proximal or Distal Locations

(A and B) Ensemble of SypHy events occurring near the membrane, i.e., the x axis position of SypHy events occurring with respect to ribbon PSF $\leq +50$ nm (A, N = 25, referred to as "proximal" events) or PSF ≥ -50 nm (B, N = 22, referred to as "distal" events). SypHy events occurring at proximal locations (A) appeared abruptly, remained at a constant level (~300 ms, green shading), and then declined. SypHy events occurring at distal locations (B) persisted longer compared with burst events (~700 ms, green shading), before decaying. For comparison, fluorescence was normalized to the peak for the individual record (See Methods).

(C and D) Decay of ensemble SypHy fluorescence for proximal (red) or distal (blue) events. Green line indicates best-fit Monte Carlo simulation with a diffusion coefficient of 49 nm^2/ms for proximal events (C) and 16.1 nm^2/ms for distal events (D).

See also Figure S5.

photobleaching (FRAP) experiments in zebrafish bipolar cells that express higher levels of SypHy in retinal bipolar cells (Odermatt et al., 2012). To do so, we measured recovery from photobleaching in a 1 × 1-μm region on the surface of bipolar cell terminals. Photobleaching resulted in a rapid drop in fluorescence, with a recovery that returned to baseline fluorescence over minutes. To extract diffusion coefficient information, we fit to the previously derived equation for 2D diffusion (Axelrod et al., 1976; Feder et al., 1996) (Figure S5):

$$F(t) = [F_0 + (R(F^0 - F_0) + F_0)(t/\tau)]/(1 + t/\tau)$$

where R represents the fraction of the mobile pool, τ is the half-time of recovery, F^0 is the fluorescence before bleaching, and F_0 is the fluorescence immediately after bleaching, and obtained best-fit values of R = .95 and τ = 5578 ms. The diffusion coefficient is determined from the equation (Gomez-Varela et al., 2010):

$$D = \text{Area of bleach}/4\tau$$

yielding an estimate of 44 nm^2/ms for D. As the vast majority of the terminal is outside the limited active zone, this primarily represents diffusion in extrasynaptic regions of the terminal.

DISCUSSION

Clearance of synaptic vesicle components following exocytosis from release sites is an important determinant of recovery from short-term synaptic depression, and the clearance and availability of release sites has been suggested to be rate limiting during sustained synaptic release (Hosoi et al., 2009; Hua et al., 2013; Wen et al., 2018; Wu et al., 2009). At the rod ribbon synapse, pharmacological blockage of dynamin-dependent endocytosis strongly reduces subsequent exocytosis without changing vesicle docking rates, suggesting that release site clearance is necessary to maintain release at these synapses (Wen et al., 2018). Nevertheless, little information has been available about the dynamics of newly fused vesicle proteins at the active zone. In the present study, we directly addressed this question using single-molecule imaging at the active zone of a living neuron and derived real-time information about the clearance of individual synaptic vesicle proteins following exocytosis. To study these processes, we monitored the fate of synaptophysin molecules following exocytosis from zebrafish bipolar cell ribbon synapses. Our results demonstrate that the clearance of synaptophysin from the synapse is influenced by the time and location of vesicle fusion and suggest a model that supports clearance of massive amount of membrane added at the beginning of a voltage step.

Synaptophysin is a synaptic vesicle protein that regulates endocytosis of synaptic vesicles during and after sustained transmission (Kwon and Chapman, 2011). Synaptophysin has also been suggested to act as a release site clearance factor, preventing synaptobrevin 2 forming *cis*-SNARE complexes from obstructing release sites (Rajappa et al., 2016). To track newly released synaptophysin, we capitalized on our ability to localize active zones using a ribbon-binding peptide (Zenisek et al., 2004). Our results differ from previous measurements of mobility of membrane proteins using single particle tracking, fluorescence recovery after photobleaching, and fluorescence correlation spectroscopy in that our approach is able to distinguish newly released protein following exocytosis. Protein diffusion is influenced by interplay of protein-to-lipid ratios (Ramadurai et al., 2009), curvature of the membrane (Leitenberger et al., 2008), membrane tension (Quemeneur et al., 2014), lipid packing (Javanainen et al., 2013), and protein shape. To our knowledge, only Gimber et al. (2015) have combined tracking newly exocytosed synaptic vesicle proteins with localizing active zone in neurons, and then only in sequentially acquired images separated by some time, which were intended to test whether observed newly exocytosed pHluorin coincided with active zone marker, Munc 13-1. By using two-color laser scanning confocal microscopy, we were able to detect the locus of fusion and track individual SypHy molecules following exocytosis during sustained depolarization using live cell imaging in voltage-clamped synaptic terminals.

Our results demonstrate that the rate of fluorescence decline and thus SypHy clearance is influenced by the timing and location of vesicle fusion at bipolar cell ribbon synapses. Our results indicate a faster apparent diffusion coefficient for burst events (41.8 nm^2/ms) compared with late events (9.6 nm^2/ms). It should be noted that this difference may be an underestimate, because longer dwell times would be expected to be contaminated to a greater degree by photobleaching. These results suggest that the burst phase of exocytosis enhances clearance from the synapse. To account for this difference, we suggest a model in which the massive amount of membrane added at the beginning of a voltage step may act to push synaptophysin and other synaptic vesicle components from the synapse. The transient component of zebrafish bipolar cells measured by capacitance measurements suggests that about 1,200 synaptic vesicles are released with a time constant of 2.3 ms (Vaithianathan and Matthews, 2014) at approximately 50 ribbon sites, an average of 24 per ribbon. On average, this burst phase would be expected to add 0.07 μm^2 of membrane per active zone assuming a vesicle diameter of 30 nm. The synaptic ribbon at the base covers a roughly rectangular region of membrane 0.4 μm long by 0.15 μm wide for an area of 0.06 μm^2 (von Gersdorff and Matthews, 1996, 1999). Hence, the burst phase of exocytosis is expected to more than double the active zone membrane in <5 ms. Ca^{2+} channels at photoreceptor synapses also exhibit increased mobility at times of high rates of exocytosis (Mercer et al., 2011), suggesting that this may be a general feature of ribbon synapses. Interestingly, unlike SypHy, Ca^{2+} channels in both bipolar cells and photoreceptors appear to be confined to a restricted region, which can be disrupted by reagents that disrupt the actin cytoskeleton (Mercer et al., 2011; Thoreson et al., 2013).

Release site clearance is likely a complex process and may be influenced by multiple factors (Haucke et al., 2011; Neher, 2010). Previous measurements of diffusion coefficients of membrane proteins have ranged from 1–300 nm^2/ms (Bannai et al., 2009; Dahan et al., 2003; Funahashi et al., 2018; Gomez-Varela et al., 2010; Groc et al., 2008; Mercer et al., 2011; Mikasova et al., 2008), placing our values of ~42 nm^2/ms during the burst phase and ~10 nm^2/ms during the sustained phase at the low end of membrane protein

measurements and much lower than the previous report on synaptophysin in hippocampal synapses (180 nm^2/ms) (Funahashi et al., 2018). We propose the following three hypotheses for why our results may differ: (1) the ribbon synapse may be more densely packed with protein and other diffusion barriers than a conventional synapse or perisynaptic regions; (2) our cells exhibit minimally expressing synaptophysin-pHluorin molecules, whereas previous measurements were maximized for visualizing release and hence exhibited a much higher concentration of released synaptophysin; if fixed synaptophysin-binding proteins reside within the active zone, binding sites may be saturated in their model allowing for free diffusion; and (3) synaptophysin may have different mobility in the membrane of fish bipolar cells than in mouse hippocampal neurons. To begin to address this issue, we used FRAP to look at the diffusion coefficient of SypHy in a different line of zebrafish with higher expression on the cell surface. Because the region immediately below the ribbon is a small fraction of the total area of the terminal, these measurements are dominated by SypHy in extrasynaptic regions. With the FRAP data, we find that the diffusion coefficient in the extrasynaptic membrane is 44 nm^2/ms, similar to burst phase around the ribbon and about 4-fold faster than when events are rare, but still much slower than results in hippocampal neurons. These results suggest that the region around the ribbon may exhibit lower protein mobility at rest than the surrounding plasma membrane. Based on these results, we suggest that the region immediately surrounding the synapse may be a region that contains a higher density of diffusion barriers that may restrict movement of molecules, but that the membrane flow associated with exocytosis may be able to overcome this restricted mobility. In addition, our results show that synaptophysin movement is more restricted in the bipolar cell than in hippocampal neurons and that transgene expression level is unlikely to account for our differences. Together our results suggest that plasma membrane structure may vary between these different types of cells and regions, because lateral diffusion is highly sensitive to protein-lipid contacts (Knight et al., 2010) and protein concentration (Goose and Sansom, 2013) and protein-to-lipid ratio varies extensively across different microstructures of biological membrane (Dupuy and Engelman, 2008).

Interestingly, studies from photoreceptor synapses (Mercer et al., 2011) and bipolar cells (Thoreson et al., 2013) found that the α2δ subunit of voltage-gated Ca^{2+} (Ca_V) channels positioned close to the synaptic ribbons exhibited diffusion within a restricted domain, but were confined to a location surrounding the active zone. Despite being embedded within a much larger complex than synaptophysin, α2δ subunits exhibited diffusion coefficients within the restricted domain of 170 nm^2/ms in photoreceptors and 300–450 nm^2/ms in bipolar cells, an order of magnitude higher than our measurements. The calcium channel measurements were accomplished by coupling α2δ subunits to quantum dots via antibodies. The superior fluorescent properties of quantum dots enable the authors to track smaller lateral movements with much higher spatial resolution than we are able to achieve with single-molecule imaging of GFP. Hence, it is possible that synaptophysin undergoes similar rapid diffusion on a local scale that goes undetected with our techniques.

Our results indicate that the dynamics of clearance is accelerated at times when exocytosis rates are high or when vesicles fuse in proximity to the plasma membrane. However, it is not clear whether the proximity of the vesicles to the plasma membrane or the overall exocytosis rate is the dominant factor in determining clearance rates. This poses an interesting avenue for future research using our approach. The dynamics of release site clearance was argued as a limiting and modulatory element in synaptic transmission. Further studies are required to determine the mode of vesicle fusion and limits of bipolar cell ribbon synapse to sustain the transmission during strong stimulation for encoding background illumination. We believe that our direct approach of imaging single vesicles (Vaithianathan et al., 2016) in conjunction with capacitance measurements and tracking clearance of fused vesicle protein demonstrated in this study are valuable tools that can be combined in the future to explore this question.

Limitations of the Study

The limitation of the study is governed by optimizing parameters to track a single molecule at a single active zone in a living terminal for several seconds. The ability to obtain such measurements is limited by several factors: the optics, health of the neuron, incorporation of the transgene, the stability of the system, the trade-off between signal-to-noise ratio (SNR), and bleaching. We acknowledge that our study could have failed to detect smaller lateral movements due to SNR, attributes to rapid diffusion demonstrated previously for other synaptic proteins.

METHODS

All methods can be found in the accompanying Transparent Methods supplemental file.

SUPPLEMENTAL INFORMATION

Supplemental Information can be found online at https://doi.org/10.1016/j.isci.2019.06.015.

ACKNOWLEDGMENTS

This work was supported by NIH grant EY003821 to G.M. and L.P.W. and EY014990 and EY021195 to D.Z. and the Yale vision core grant EY026878. The authors thank Dr. Leon Lagnado (University of Sussex) for the Ribeye: sypHy line of zebrafish.

AUTHOR CONTRIBUTIONS

T.V. and G.M. conceived research goals and aims. T.V designed and collected data for all experiments, analyzed, prepared images, and wrote the paper. D.Z. helped with analysis, expertise feedback, creation of models, review, and editing. L.P.W. helped with image preparation, software, review, and editing. D.H. cloned synaptophysin-pHluorin fusion protein. T.V. and D.H. generated synaptophysin-pHluorin transgenic zebrafish.

DECLARATION OF INTERESTS

The authors declare no competing interests.

Received: August 21, 2018
Revised: September 13, 2018
Accepted: June 7, 2019
Published: July 26, 2019

REFERENCES

Axelrod, D., Koppel, D.E., Schlessinger, J., Elson, E., and Webb, W.W. (1976). Mobility measurement by analysis of fluorescence photobleaching recovery kinetics. Biophys. J. *16*, 1055–1069.

Balaji, J., and Ryan, T.A. (2007). Single-vesicle imaging reveals that synaptic vesicle exocytosis and endocytosis are coupled by a single stochastic mode. Proc. Natl. Acad. Sci. U S A *104*, 20576–20581.

Bannai, H., Levi, S., Schweizer, C., Inoue, T., Launey, T., Racine, V., Sibarita, J.B., Mikoshiba, K., and Triller, A. (2009). Activity-dependent tuning of inhibitory neurotransmission based on GABAAR diffusion dynamics. Neuron *62*, 670–682.

Dahan, M., Levi, S., Luccardini, C., Rostaing, P., Riveau, B., and Triller, A. (2003). Diffusion dynamics of glycine receptors revealed by single-quantum dot tracking. Science *302*, 442–445.

Dupuy, A.D., and Engelman, D.M. (2008). Protein area occupancy at the center of the red blood cell membrane. Proc. Natl. Acad. Sci. U S A *105*, 2848–2852.

Feder, T.J., Brust-Mascher, I., Slattery, J.P., Baird, B., and Webb, W.W. (1996). Constrained diffusion or immobile fraction on cell surfaces: a new interpretation. Biophys. J. *70*, 2767–2773.

Funahashi, J., Tanaka, H., and Hirano, T. (2018). Visualization of synchronous or asynchronous release of single synaptic vesicle in active-zone-like membrane formed on neuroligin-coated glass surface. Front. Cell. Neurosci. *12*, 140.

Gimber, N., Tadeus, G., Maritzen, T., Schmoranzer, J., and Haucke, V. (2015). Diffusional spread and confinement of newly exocytosed synaptic vesicle proteins. Nat. Commun. *6*, 8392.

Gomez-Varela, D., Kohl, T., Schmidt, M., Rubio, M.E., Kawabe, H., Nehring, R.B., Schafer, S., Stuhmer, W., and Pardo, L.A. (2010). Characterization of Eag1 channel lateral mobility in rat hippocampal cultures by single-particle-tracking with quantum dots. PLoS One *5*, e8858.

Goose, J.E., and Sansom, M.S. (2013). Reduced lateral mobility of lipids and proteins in crowded membranes. PLoS Comput. Biol. *9*, e1003033.

Granseth, B., Odermatt, B., Royle, S.J., and Lagnado, L. (2006). Clathrin-mediated endocytosis is the dominant mechanism of vesicle retrieval at hippocampal synapses. Neuron *51*, 773–786.

Groc, L., Choquet, D., and Chaouloff, F. (2008). The stress hormone corticosterone conditions AMPAR surface trafficking and synaptic potentiation. Nat. Neurosci. *11*, 868–870.

Haucke, V., Neher, E., and Sigrist, S.J. (2011). Protein scaffolds in the coupling of synaptic exocytosis and endocytosis. Nat. Rev. Neurosci. *12*, 127–138.

Hosoi, N., Holt, M., and Sakaba, T. (2009). Calcium dependence of exo- and endocytotic coupling at a glutamatergic synapse. Neuron *63*, 216–229.

Hua, Y., Woehler, A., Kahms, M., Haucke, V., Neher, E., and Klingauf, J. (2013). Blocking endocytosis enhances short-term synaptic depression under conditions of normal availability of vesicles. Neuron *80*, 343–349.

Javanainen, M., Hammaren, H., Monticelli, L., Jeon, J.H., Miettinen, M.S., Martinez-Seara, H., Metzler, R., and Vattulainen, I. (2013). Anomalous and normal diffusion of proteins and lipids in crowded lipid membranes. Faraday Discuss. *161*, 397–417, discussion 419–459.

Knight, J.D., Lerner, M.G., Marcano-Velazquez, J.G., Pastor, R.W., and Falke, J.J. (2010). Single molecule diffusion of membrane-bound proteins: window into lipid contacts and bilayer dynamics. Biophys. J. *99*, 2879–2887.

Kwon, S.E., and Chapman, E.R. (2011). Synaptophysin regulates the kinetics of synaptic vesicle endocytosis in central neurons. Neuron *70*, 847–854.

Leitenberger, S.M., Reister-Gottfried, E., and Seifert, U. (2008). Curvature coupling dependence of membrane protein diffusion coefficients. Langmuir *24*, 1254–1261.

Matthews, G., and Fuchs, P. (2010). The diverse roles of ribbon synapses in sensory neurotransmission. Nat. Rev. Neurosci. *11*, 812–822.

Mennerick, S., and Matthews, G. (1996). Ultrafast exocytosis elicited by calcium current in synaptic terminals of retinal bipolar neurons. Neuron *17*, 1241–1249.

Mercer, A.J., Chen, M., and Thoreson, W.B. (2011). Lateral mobility of presynaptic L-type calcium channels at photoreceptor ribbon synapses. J. Neurosci. *31*, 4397–4406.

Mikasova, L., Groc, L., Choquet, D., and Manzoni, O.J. (2008). Altered surface trafficking of presynaptic cannabinoid type 1 receptor in and out synaptic terminals parallels receptor

desensitization. Proc. Natl. Acad. Sci. U S A *105*, 18596–18601.

Neher, E. (2010). What is rate-limiting during sustained synaptic activity: vesicle supply or the availability of release sites. Front. Synaptic Neurosci. *2*, 144.

Odermatt, B., Nikolaev, A., and Lagnado, L. (2012). Encoding of luminance and contrast by linear and nonlinear synapses in the retina. Neuron *73*, 758–773.

Quemeneur, F., Sigurdsson, J.K., Renner, M., Atzberger, P.J., Bassereau, P., and Lacoste, D. (2014). Shape matters in protein mobility within membranes. Proc. Natl. Acad. Sci. U S A *111*, 5083–5087.

Rajappa, R., Gauthier-Kemper, A., Boning, D., Huve, J., and Klingauf, J. (2016). Synaptophysin 1 clears Synaptobrevin 2 from the presynaptic active zone to prevent short-term depression. Cell Rep. *14*, 1369–1381.

Ramadurai, S., Holt, A., Krasnikov, V., van den Bogaart, G., Killian, J.A., and Poolman, B. (2009). Lateral diffusion of membrane proteins. J. Am. Chem. Soc. *131*, 12650–12656.

Royle, S.J., Granseth, B., Odermatt, B., Derevier, A., and Lagnado, L. (2008). Imaging phluorin-based probes at hippocampal synapses. Methods Mol. Biol. *457*, 293–303.

Sankaranarayanan, S., De Angelis, D., Rothman, J.E., and Ryan, T.A. (2000). The use of pHluorins for optical measurements of presynaptic activity. Biophys. J. *79*, 2199–2208.

Thoreson, W.B., Mercer, A.J., Cork, K.M., and Szalewski, R.J. (2013). Lateral mobility of L-type calcium channels in synaptic terminals of retinal bipolar cells. Mol. Vis. *19*, 16–24.

Vaithianathan, T., Henry, D., Akmentin, W., and Matthews, G. (2016). Nanoscale dynamics of synaptic vesicle trafficking and fusion at the presynaptic active zone. Elife *5*, 1–14.

Vaithianathan, T., and Matthews, G. (2014). Visualizing synaptic vesicle turnover and pool refilling driven by calcium nanodomains at presynaptic active zones of ribbon synapses. Proc. Natl. Acad. Sci. U S A *111*, 8655–8660.

Voglmaier, S.M., Kam, K., Yang, H., Fortin, D.L., Hua, Z., Nicoll, R.A., and Edwards, R.H. (2006). Distinct endocytic pathways control the rate and extent of synaptic vesicle protein recycling. Neuron *51*, 71–84.

von Gersdorff, H., and Matthews, G. (1994). Dynamics of synaptic vesicle fusion and membrane retrieval in synaptic terminals. Nature *367*, 735–739.

von Gersdorff, H., and Matthews, G. (1996). Calcium-dependent inactivation of calcium current in synaptic terminals of retinal bipolar neurons. J. Neurosci. *16*, 115–122.

von Gersdorff, H., and Matthews, G. (1999). Electrophysiology of synaptic vesicle cycling. Annu. Rev. Physiol. *61*, 725–752.

Wen, X., Van Hook, M.J., Grassmeyer, J.J., Wiesman, A.I., Rich, G.M., Cork, K.M., and Thoreson, W.B. (2018). Endocytosis sustains release at photoreceptor ribbon synapses by restoring fusion competence. J. Gen. Physiol. *150*, 591–611.

Wu, X.S., McNeil, B.D., Xu, J., Fan, J., Xue, L., Melicoff, E., Adachi, R., Bai, L., and Wu, L.G. (2009). Ca(2+) and calmodulin initiate all forms of endocytosis during depolarization at a nerve terminal. Nat. Neurosci. *12*, 1003–1010.

Zenisek, D., Horst, N.K., Merrifield, C., Sterling, P., and Matthews, G. (2004). Visualizing synaptic ribbons in the living cell. J. Neurosci. *24*, 9752–9759.

ISCI, Volume *17*

Supplemental Information

Tracking Newly Released Synaptic Vesicle Proteins at Ribbon Active Zones

Thirumalini Vaithianathan, Lonnie P. Wollmuth, Diane Henry, David Zenisek, and Gary Matthews

Supplemental materials

Transparent Methods

Transgenic animals

Sparse expressing adult HSP70::SypHy Zebrafish (Vaithianathan et al., 2016) of both sexes were incubated in water bath at 37°C for 2 hours one day prior to experiments to drive protein expression via the HSP70 promoter. A line of fish generated in the same manner had higher expression and were used for the experiment in Figure 5B. Animals were maintained according to NIH guidelines and all procedures were approved by the Institutional Animal Care and Use Committee of the State University of New York at Stony Brook.

For FRAP experiments (Figure S5), a transgenic line of zebrafish, kindly donated by Dr. Leon Lagnado (University of Sussex) that express SypHy off of the Ribeye A promoter (Ribeye::sypHy) were used (Odermatt et al., 2012).

Electrophysiology and analysis

Dissociation of zebrafish retinal bipolar cells: The procedure for isolating bipolar neurons from zebrafish retina was as described previously (Vaithianathan et al., 2013a). Briefly, retinas were dissected from the eyecups, treated for 25 min with hyaluronidase (1100 units/ml), cut into small pieces, and incubated 15-40 min in saline [(in mM) 115 NaCl, 2.5 KCl, 0.5 $CaCl_2$, 1 $MgCl_2$, 10 HEPES, 10 Glucose, pH 7.4], containing DL-cysteine and 15-30 units/ml papain (Sigma) at 25 ºC for 30~40 min. A piece of retina was gently triturated using a fire-polished glass Pasteur pipette and dissociated cells were plated onto glass-bottomed dishes containing a saline solution

(Heidelberger and Matthews, 1992) with $CaCl_2$ increased to 2.5 mM. ON bipolar cells were identified by their characteristic morphology.

Bipolar cell voltage clamp recordings: Whole-cell patch-clamp recordings were made from acutely dissociated bipolar cells by directly placing the patch pipette on the synaptic terminal (Vaithianathan et al., 2013b). The patch pipette solution consisted of (in mM): 120 Cs-gluconate, 10 tetraethylammonium-Cl, 3 $MgCl_2$, 0.2 *N*-methyl-d-glucamine-EGTA, 2 Na_2ATP, 0.5 Na_2GTP, 20 HEPES, pH 7.2. and bath solutions (saline, with 2.5 mM $CaCl_2$). The patch pipette solution included fluorescent RBP peptide (deep-red CF633-RBP) to mark ribbons (Zenisek et al., 2004), and 3 mM reduced glutathione as a free-radical scavenger. Membrane currents were recorded under voltage clamp using a HEKA EPC-9 amplifier controlled by PatchMaster software (HEKA). For all recordings, the holding potential was -60 or -65 mV and stepped to -10 mV (t_0) for 1s. Membrane capacitance, series conductance, and membrane conductance were measured using the sine DC method of the PatchMaster lock-in extension and a 1600 Hz sinusoidal stimulus with peak-to-peak amplitude of 10 mV centered on the holding potential (Vaithianathan et al., 2013b). Pipettes were coated with dental wax to reduce stray capacitance.

Image collection

Confocal images were acquired using Olympus FluoView software controlling an Olympus FV1000/IX-81 laser-scanning confocal microscope equipped with a 60X 1.42 NA oil-immersion objective. For experiments monitoring global SypHy responses to sustained depolarization, x-y raster scans of a zoomed terminal were acquired with scan speed of 2 μs/pixel (frame size, 256 × 256 pixels). For these experiments, bipolar terminals were stimulated at 30-s interval. Terminals with leak current >20 pA were not included in analysis.

For the vast majority of our experiments, we generated rapid x-t line scans of a zoomed region through a selected ribbon to monitor green (SypHy) fluorescence. These x-t line scans were of a duration of 1-8 msecs. To avoid potential errors arising from high curvature near the top of the terminal and the plane of adherence of the membrane to the glass coverslip at the bottom of the terminal, we carefully adjusted the focal plane to bring labeled ribbons into sharp focus. This procedure minimized curvature of the plasma membrane in the z-axis within the optical section and therefore facilitated localization of the plasma membrane with respect to the ribbon. Quantitative image analysis was performed by importing FluoView images of x-y and x-t scans into ImageJ (imagej.nih.gov) for initial processing and analysis. Subsequent analysis was performed in Igor Pro (Wavemetrics, Portland OR) using custom-written routines. Timing between voltage-clamp recording and imaging was synched by generating a horizontal-scan synch pulse by the hardware of the confocal microscope, in parallel with the voltage-clamp data (PatchMaster).

We confirmed for possible bleed-through before conducting experiments by imaging each channel with both lasers in the same imaging parameters used for experiments in bipolar cells isolated from wild-type zebrafish. To test the bleed-through from RBP channel (LD 635) to SypHy Channel (LD 488) we patched wild-type bipolar cells with patch pipette solution included fluorescent RBP peptide (deep-red CF633-RBP) to mark ribbons, performed line-scan images and analyzed in the same manner will be used for experiments. To look for possible bleed through from SypHy channel to RBP channel we followed the same procedure for GFP molecules.

Photobleaching: To minimize photobleaching and phototoxicity during live-cell imaging, we used fast scan speed (2~10 μs/pixel), low laser intensity (0.1–0.5% of maximum), and low pixel

density (frame size, 256 × 256 pixels). Photo bleaching with our imaging parameters were estimated using immobilized GFP. x-t line scans of immobilized GFP using these same imaging parameters.

Image analysis

Analysis of x-y scans: SypHy responses in x-y scans were identified using 'Image Calculator" (imagej.nih.gov) to identify loci of stimulus-dependent increases of SypHy fluorescence across the terminal. To increase the overall intensity and to improve the signal to noise ratio (SNR), we increased the pinhole. Increasing the pinhole extended the z-axis resolution to 10 μm as it collects signal from layers outside the focal plane. Square ROIs (1 x 1 μm) were then positioned at such exocytic hotspots, confirmed by RBP fluorescence, revealing active synapses. Changes in fluorescence were quantified by subtracting a three-frame average obtained immediately before depolarization from a comparable average obtained during the sustained depolarization. The recovery or decay back to baseline phase were fitted to declining exponential.

Analysis of x-t scans: SypHy Zebrafish sparsely express SypHy (Vaithianathan et al., 2016). We recorded a total of 1453 x-t line scans in response to sustained depolarization from different ribbons, and 36 line scans without membrane depolarization (controls). This data set was collected from about 1200 different terminals since in some instances we recorded from different ribbons in the same terminal. To detect a SypHy event, in a x-t line scan, we initially examined the temporal profile of x-t line around the region of interest (ROI) encompassing the ribbon and cell interior (Figure S1). We identified 81 putative SypHy events that demonstrated an increase in green fluorescence over baseline. We imaged 27-nm beads and GFP (kind gift from Dr. Mark Bowen, Stony Brook University) fixed on the glass bottom dish used for experiment

using streptavidin and biotin with the same imaging parameters used to detect SypHy events. To quantify these events, we performed single molecule image analysis:

Single molecule image analysis

x-t scans were performed at rates that varied from 125 to 1,000 Hz. To optimize quantification of RBP and SypHy fluorescence, we averaged x-t images over 2 pixels in the x-axis and 5-8 lines in the t-axis. In some instances, as delineated below, we further averaged the images.

x-axis profile: To determine the location of SypHy events with respect to ribbon location, we fit x-axis intensity profiles with the equation $f(x) = s(x) + g(x)$ (Vaithianathan et al., 2016). Here, $s(x)$ is a sigmoid describing the transition from intracellular to extracellular background fluorescence at the edge of the cell, given by $s(x) = b- (c/(1-\exp((x_{1/2}-x)/d)))$, and $g(x)$ is a Gaussian representing the fluorescence of RBP and SypHy, given by $g(x) = a(\exp(-(x-x0)^2/w^2))$. The parameters $x_{1/2}$ and x_0 were taken as the x-axis positions of the plasma membrane and the fluorescence emitter, respectively. The parameter b is intracellular background fluorescence, c is extracellular background fluorescence, d is the slope factor of the sigmoid, a is the peak amplitude of emitter fluorescence, and w is $\sqrt{2}$* the standard deviation of the Gaussian. In practice, the latter parameters were highly constrained by the data or by the measured PSF, essentially leaving only $x_{1/2}$ and x_0 as free parameters in the fitting.

Analysis along t-axis profile

To compare SypHy events obtained from different experiments, we defined several parameters:

Event amplitude: To measure the amplitude of SypHy events, we took the difference between the 'peak' amplitude of the SypHy event and the baseline, the average fluorescence obtained

immediately before depolarization. To measure the 'peak' amplitude, we identified the maximum value that occurred early during the SypHy event and averaged 5 points centered around the peak. To define the limits of small amplitude events, we randomly chose 203 out of 1372 null events and measured 'event amplitudes' by taking the difference between average fluorescence immediately after the depolarization and the baseline, averaging 5 points.

To evaluate the imaging noise, measurements were obtained using the same approach as with SypHy and nulls except that noise measurements were made in the absence of a stimulus (N=36). The results were normalized to the total number of trials and fit with Gaussian function red (red; σ=4.9.

Point spread function (PSF): To characterize the PSF, we used the full width at half maximum (FWHM) (citation). The lateral and axial point spread function is obtained by taking an XYZ scan through a single 27 nm bead. The maximum projection in the xy-plane was fit to the Gaussian function, $g(x,y) = z\_0 + [(-1)/2(1 - \ 〚cor〛\ ^2\ )\ (((x - x\_0)/xwidth)^2 + ((y - y\_0)/ywidth)^2 - 2cor(x - x\_0\ )(y - y\_0\ )/(xwidth \cdot ywidth))]$ to obtain the lateral resolution (FWHM). Similarly, the y-z axis projection was fit to the Gaussian function, $g(y,z) = z\_0 + [(-1)/2(1 - \ 〚cor〛\ ^2\ )\ (((y - y\_0)/ywidth)^2 + ((z - z\_0)/zwidth)^2 - 2cor(y - y\_0\ )(z - z\_0\ )/(ywidth \cdot zwidth))]$ to obtain the axial resolution. FWHMs that we obtained from x-width was 259 nm in the lateral (x-y plane) and y-z-width was 448 nm in the axial (y-z axis) resolution.

To determine the FWHM of SypHy events, we fit x-axis intensity profiles with the equation f(x) = s(x) + g(x) (Vaithianathan et al., 2016). Here, s(x) is a sigmoid describing the transition from intracellular to extracellular background fluorescence at the edge of the cell, given by s(x) = b- (c/(1-exp(($x_{1/2}$-x)/d))), and g(x) is a Gaussian representing the fluorescence of

SypHy, given by $g(x) = a(\exp(-(x-x0)^2/w^2))$. The parameters $x_{1/2}$ and x_0 were taken as the x-axis positions of the plasma membrane and the fluorescence emitter, respectively. Here the parameter w (width) is √2* the standard deviation of the Gaussian, which we used to determine the FWHM.

Event onset: To determine the time of SypHy event occurrence, referred to as t_1, we identified the time when the SypHy fluorescence reached 10% of the event amplitude. Due to noisiness of the traces, the 10% value was often difficult to define. In such cases, traces were subjected to additional temporal averaging to estimate event timing.

Dwell time: SypHy events remain at fusion sites with different durations before declining to baseline fluorescence. We refer this period as event duration or dwell time, which we quantified by measuring the duration between the time of SypHy event occurrence (t_1), to fluorescence decline to 1σ (68%) of event amplitude.

Ensemble averages: To categorize SypHy events we grouped the averaged records as following: we initially generated a common time base (10 ms sample interval) by interpolating values using IGOR Pro and aligned to start of event onset. Resulting events were grouped into different categories after normalizing to their event amplitude. To compare SypHy events occurring during burst vs. sustained component of release, we grouped SypHy events occurring within 30 ms from start of depolarization or 500 ms after onset of depolarization.

For locus of vesicle fusion, we grouped SypHy events based on the location relative to the center of the ribbon in the x-dimension (x_0 defined above)***;*** SypHy events that occurred at $x_0 > 50$ nm and $x_0 < -50$ nm were classified as membrane proximal and distal events, respectively.

Simulation of the random-walk of single molecules.

We performed Monte Carlo simulations of a molecule undergoing a 2D random walk illuminated by a line scan. The random-walk was constructed for 84 single-molecule diffusion trajectories using a routine written in Excel. By convolving the location of the molecule to Gaussian function with the spatial (x-axis), and axial (z-axis) PSF of the microscope, we were able to determine the expected change in fluorescence as a function of time for clearance of SypHy molecules by diffusion for various diffusion coefficients (D). A best-fit was determined by varying D to minimize the squared difference between the observed and simulated curves.

Statistical methods

No statistical method was used to predetermine sample size. Variance in estimates of the population mean is reported as ± sem. Statistical significance of differences in average amplitudes of rare and evoked events was assessed using unpaired, two-tailed *t* tests with unequal variance.

Supplemental Figure legends

Figure S1, relates to Figure 1. Analysis of SypHy fluorescence along t-axis.
(A) ***Upper***, Raw x-t raster plot, obtained at 2.36 ms/line consisting of 1026-line scans, showing t-axis intensity profiles of SypHy fluorescence (green) during sustained depolarization (same record as in Figure 1). The ROI, the area between the two white dashed lines, was obtained from the raw x-axis intensity profile (B, green).
Lower, Same line scan as in A but averaged, using the integration function in ImageJ, over 2-pixels along the x-axis and 5 scan lines along the time axis to enhance the SypHy fluorescence signal. The two dashed lines indicate the ROI, obtained in the same manner explain for raw line scan. The spatial profile for averaged line-scan is shown in *A, middle-black* trace.
(B) Spatial (x-axis) intensity profile of x-t raster scan, either the raw (green) or averaged (black) scan in A. The green dash line is centroid (x_0) of the Gaussian fit of the SypHy fluorescence. The black (white lines in A) lines are ± 1 σ of the centroid and were used to define the ROI in upper scan in A. Spatial profiles were obtained as in Figure 1C.
(C) Temporal (t-axis) intensity profile of SypHy fluorescence taken from the ROI either for the raw (green, upper scan in A) or averaged (black, lower scan in A) scan. The scans were similar in overall shape and magnitude, but the averaged scan allowed for more quantitative analysis.

Figure S2, relates to Figure 1: Spatial distribution of SypHy events.
Histogram of the x-axis position of 81 SypHy events during sustained depolarization. The relative position of the plasma membrane (solid arrow) and membrane curvature (dashed arrow) were obtained as described previously (Vaithianathan et al., 2016).

Figure S3, relates to Figure 2. Evidence for single molecule imaging.
(**A**) Example of a SypHy event (arrow) that occurred at a time > 4 s after the end of the depolarizing step (t_1). SypHy events unrelated to the depolarizing step, occurring 4 s after the end or before the depolarizing step, are classified as rare events. A total of 6 SypHy events were classified as rare.
(**B**) Average amplitudes of rare (25.2 ± 4.9, N = 6) and evoked (and 27.1 ± 1.2, N = 75) events. Values are not statistically different (*t-test*, $p < 0.05$).
(**C**) The PSF of a 27-nm fluorescence bead (black). The PSF was obtained from the fit with a Gaussian function and were quantified using the full width at half maximum (FWHM) (see Materials & Methods).
(**D**) ***Left,*** Spatial profile comparison of a single 27-nm bead (C) with SypHy fluorescence (D) derived from x-t line scans. One-dimensional Gaussian fitted to x-t line scans of a single 27-nm bead or Sigmoid-Gaussian fitted SypHy fluorescence by using Igor Pro. The indicated width (0.14 ± 0.2 μm, N = randomly chose 3 out of 81 SypHy events) of the spatial profile of SypHy fluorescence obtained from the Sigmoid-Gaussian fit (see Materials & Methods; Figure 1C) matches the width of a single 27-nm bead (0.12 ± 0.2 μm, N = 4).
Right, Scatter plot of spatial profile of SypHy fluorescence obtained from the Sigmoid-Gaussian fit. Average width (blue diamond), 0.14 ± 0.03 μm; N = 40. Note, we limited this analysis to only the brighter SypHy events, since those would be the most likely to arise from multiple molecules.

Figure S4, relates to Figure 2. Decay kinetics are independent of event amplitude.
(**A**) Average of SypHy events with amplitudes above 30 a.u. (A, black line; N = 36) or below 20 a.u. (A, gray line; N = 33). Scans were aligned to event onset and normalized to their event amplitude.
(**B**) Scatter plot of event amplitude (pA) vs. dwell time (ms) of all events (N = 81). The dash line (blue) show the best fit (r = –0.3)

Figure S5, relates to Figure 7. Fluorescence recovery after photobleaching. Average fluorescence from 18 1 μm x 1 μm square region showing recovery after being subjected to intense light (21.6 ms) to induce photobleaching. Red line represents best-fit to a 2D diffusion model (Axelrod et al., 1976).

Supplemental Figures

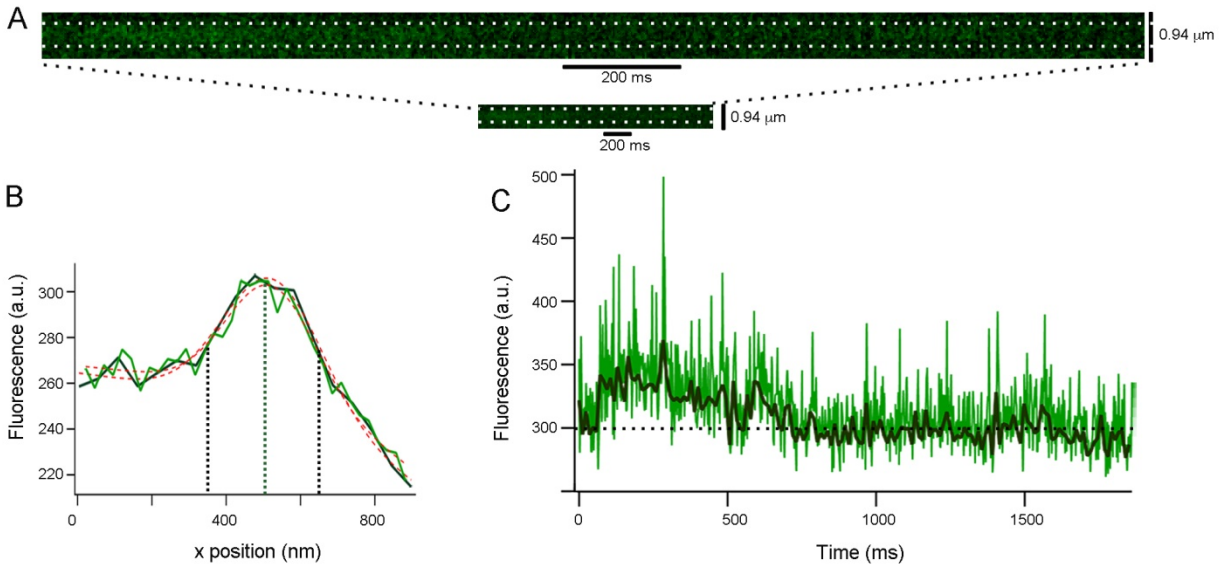

Figure S1, relates to Figure 1. Analysis of SypHy fluorescence along t-axis.

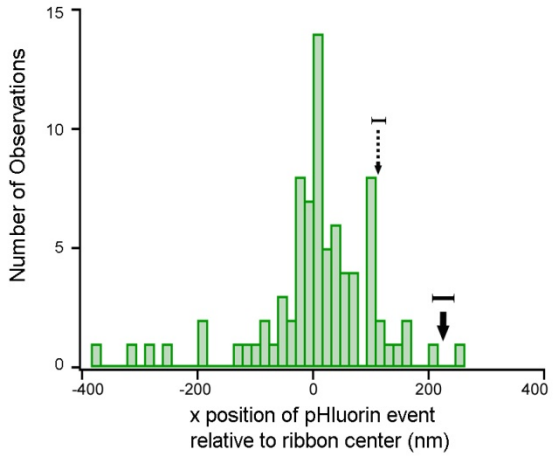

Figure S2, relates to Figure 1: Spatial distribution of SypHy events.

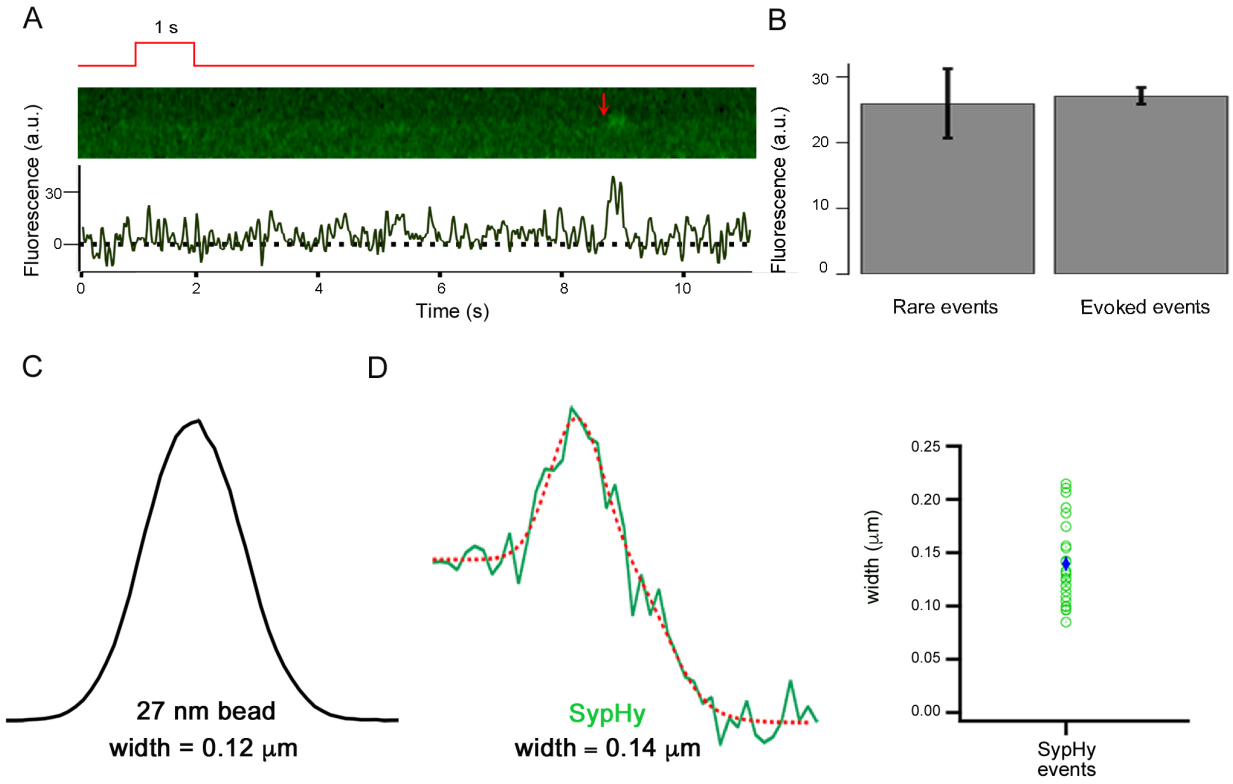

Figure S3, relates to Figure 2. Evidence for single molecule imaging.

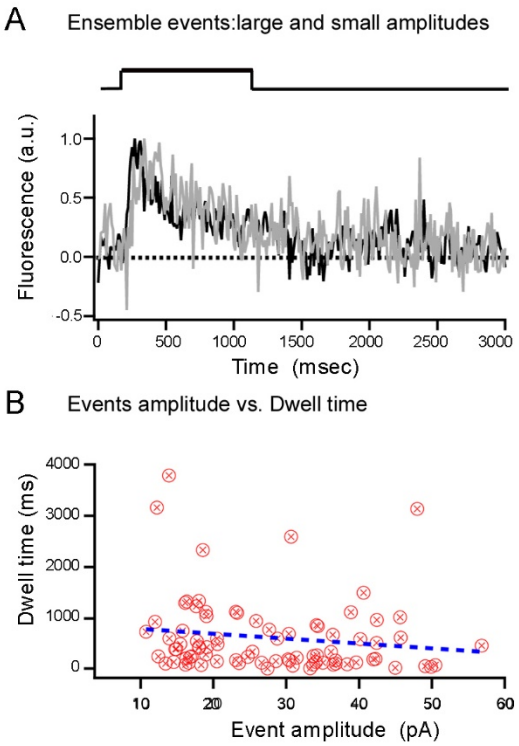

Figure S4, relates to Figure 2. Decay kinetics are independent of event amplitude.

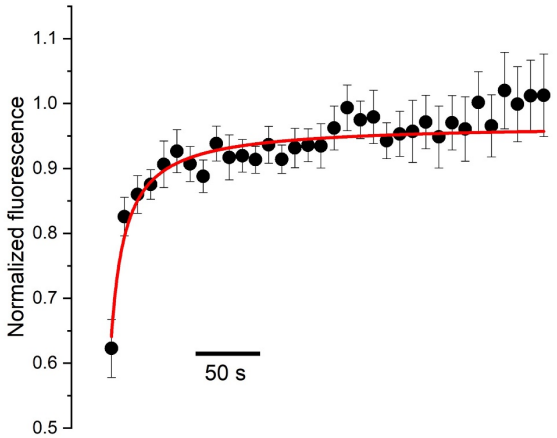

Figure S5, relates to Figure 7. Fluorescence recovery after photobleaching.

Supplemental References

Axelrod, D., Koppel, D.E., Schlessinger, J., Elson, E., and Webb, W.W. (1976). Mobility measurement by analysis of fluorescence photobleaching recovery kinetics. Biophys J *16*, 1055-1069.
Heidelberger, R., and Matthews, G. (1992). Calcium influx and calcium current in single synaptic terminals of goldfish retinal bipolar neurons. J Physiol *447*, 235-256.
Odermatt, B., Nikolaev, A., and Lagnado, L. (2012). Encoding of luminance and contrast by linear and nonlinear synapses in the retina. Neuron *73*, 758-773.
Vaithianathan, T., Akmentin, W., Henry, D., and Matthews, G. (2013a). The ribbon-associated protein C-terminal-binding protein 1 is not essential for the structure and function of retinal ribbon synapses. Mol Vis *19*, 917-926.
Vaithianathan, T., Henry, D., Akmentin, W., and Matthews, G. (2016). Nanoscale dynamics of synaptic vesicle trafficking and fusion at the presynaptic active zone. Elife *5*.
Vaithianathan, T., Zanazzi, G., Henry, D., Akmentin, W., and Matthews, G. (2013b). Stabilization of spontaneous neurotransmitter release at ribbon synapses by ribbon-specific subtypes of complexin. J Neurosci *33*, 8216-8226.
Zenisek, D., Horst, N.K., Merrifield, C., Sterling, P., and Matthews, G. (2004). Visualizing synaptic ribbons in the living cell. J Neurosci *24*, 9752-9759.